Supporting Information:

A Droplet-Based Microfluidics Route to Temperature-Responsive Colloidal Molecules

Feifei Peng,[†,‡,⊥] Linda K. Månsson,[†,‡,⊥] Stefan H. Holm,[¶,‡,⊥] Somnath Ghosh,[†,‡] Göran Carlström,[§] Jérôme J. Crassous,[†,‡,#] Peter Schurtenberger,[*,†,‡,‖] and Jonas O. Tegenfeldt[*,¶,‡]

†*Division of Physical Chemistry, Lund University, SE-22100 Lund, Sweden*

‡*NanoLund, SE-22100 Lund, Sweden*

¶*Division of Solid State Physics, Lund University, SE-22100 Lund, Sweden*

§*Centre for Analysis and Synthesis, Lund University, SE-22100 Lund, Sweden*

‖*Lund Institute of advanced Neutron and X-ray Science (LINXS), Lund University, SE-22370 Lund, Sweden*

⊥*These authors contributed equally to this work*

#*Current address: Institute of Physical Chemistry, RWTH Aachen University, 52074 Aachen, Germany*

E-mail: peter.schurtenberger@fkem1.lu.se; jonas.tegenfeldt@ftf.lth.se

Microgel Synthesis and Functionalization

PNIPAM-*co*-AAc Microgels

NIPAM (97%, Aldrich, 3.0 g), BIS (99%, Sigma-Aldrich, 0.21 g, 5 mol% with respect to NIPAM), and MRB (Polysciences Inc., 3.0 mg) were stirred in Milli-Q water (150 ml) for 40 min at 60 °C and with nitrogen purging before increasing the temperature to 80 °C. At 80 °C, a solution of KPS (≥99%, Sigma-Aldrich, 51 mg in 20 ml of Milli-Q water) was added drop-wise, followed by a solution of AAc (99.5%, Acros organics, 400 μl, 22 mol% with respect to NIPAM, in 10 ml of Milli-Q water). The reaction was allowed to proceed for 4 h under stirring (500 rpm) before cooling down to room temperature. The microgel suspension was filtered through glass wool to remove traces of coagulum, and was thereafter purified by repeated cycles of centrifugation, decantation and redispersion.

PNIPMAM-*co*-AAc Microgels

NIPMAM (97%, Aldrich, 3.0 g), BIS (0.18 g, 5 mol% with respect to NIPMAM), SDS (>99%, Duchefa Biochemie, 13 mg) and a FITC solution (prepared by reacting FITC (>90%, Sigma, 34 mg) and allylamine (AL, 98%, Aldrich, 35 μl) in a NaOH solution (10 ml, 10^{-4} M)) were stirred in Milli-Q water (132 ml) for 25 min at room temperature and with nitrogen purging before increasing the temperature to 80 °C. At 80 °C, a solution of KPS (51 mg in 5 ml of Milli-Q water) was added drop-wise, followed by a solution of AAc (355 μl, 22 mol% with respect to NIPMAM, in 10 ml of Milli-Q water). The reaction was allowed to proceed for 3 h with stirring (500 rpm) before cooling down to room temperature. The microgel suspension was filtered through glass wool to remove traces of coagulum and was thereafter purified by dialysis for 2 weeks.

PNIP(M)AM-GMA Microgels

HCl solution (2 M, 100 μl/100 g of microgel suspension) and GMA (97%, Aldrich, 1.2 ml/100 g of microgel suspension) were added to a 1 wt% PNIP(M)AM-*co*-AAc suspension under stirring (500 rpm). Stirring was continued for 30 min at room temperature, before increasing the temperature to 50 °C. Reactions were allowed to proceed for 24 h before cooling down. The suspensions were filtered through glass wool and were then purified by means of repeated cycles of centrifugation, decantation and redispersion.

GMA-functionalization was confirmed by ^{1}H NMR spectroscopy (Fig. S1), through the appearance of peaks corresponding to the vinyl (=CH_2) protons of GMA. Prior to NMR, the microgel suspensions were extensively dialysed in order to ensure removal of impurities such as unreacted GMA. Upon dialysis, the suspensions were freeze-dried and the microgels were then redispersed in D_2O to yield suspensions of 1 wt%. Spectra are shown in Fig. S1. For a complete peak assignment, please refer to reference.[1]

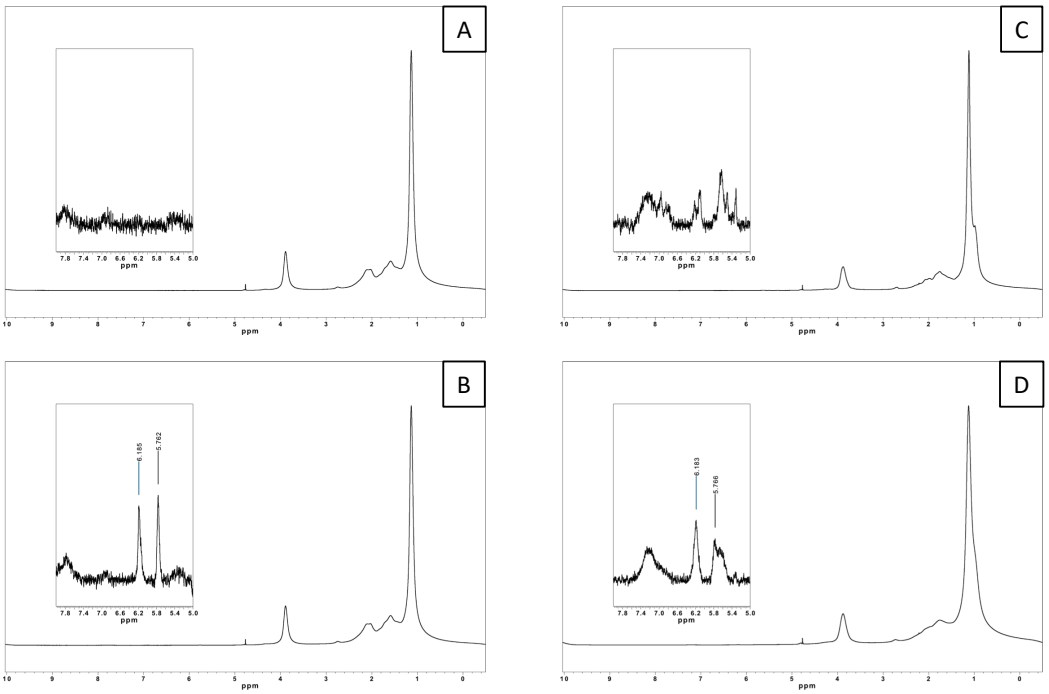

Figure S1: 600 MHz 1D ^{1}H-NMR spectra (D_2O) of **(A)** PNIPAM-*co*-AAc, **(B)** PNIPAM-GMA, **(C)** PNIPMAM-*co*-AAc and **(D)** PNIPMAM-GMA. Insets show the 5.0-8.0 ppm region, with peaks corresponding to the vinyl protons of GMA labelled.

PNIP(M)AM-*co*-AL Microgels

Using literature procedures,[2,3] NIP(M)AM, BIS (5 mol% with respect to NIP(M)AM) and allylamine (AL, 10 mol%) were co-polymerised to prepare PNIP(M)AM-*co*-AL microgels. KPS was used as initiator and SDS as stabiliser. Interparticle crosslinking through coupling of the microgels' amine groups could be affected using GDA (50 wt%, Aldrich) (Fig. S2A): stable, thermoresponsive macrogels (Fig. S2B) were prepared by addition of GDA solution to dense microgel pellets prepared by centrifugation.

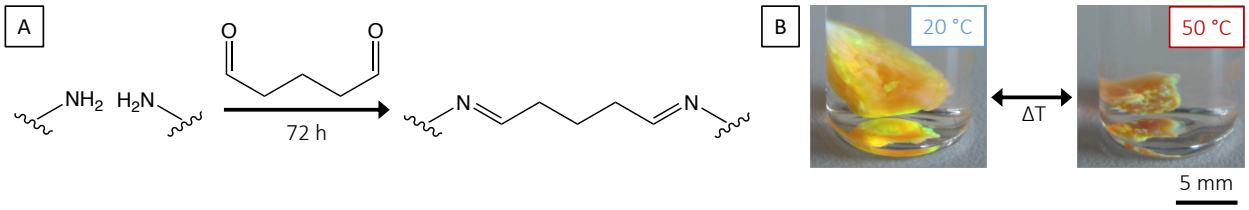

Figure S2: **(A)** Reaction scheme for microgel-microgel crosslinking of PNIP(M)AM-*co*-AL microgels using GDA. **(B)** Stable macrogels based on PNIP(M)AM-*co*-AL microgels shrink reversibly when crossing the VPTT.

Reversibility of Gelation in Microgel Suspensions

Below the VPTT, PNIP(M)AM-GMA suspensions possess liquid behavior (Fig. S3). Crossing of the VPTT is characterized by the formation of a gel that forms as a response to the repulsive-to-attractive transition experienced by the microgels. The liquid-to-gel transition is completely reversible, as evidenced by the return to a liquid state on cooling down to temperatures below the VPTT.

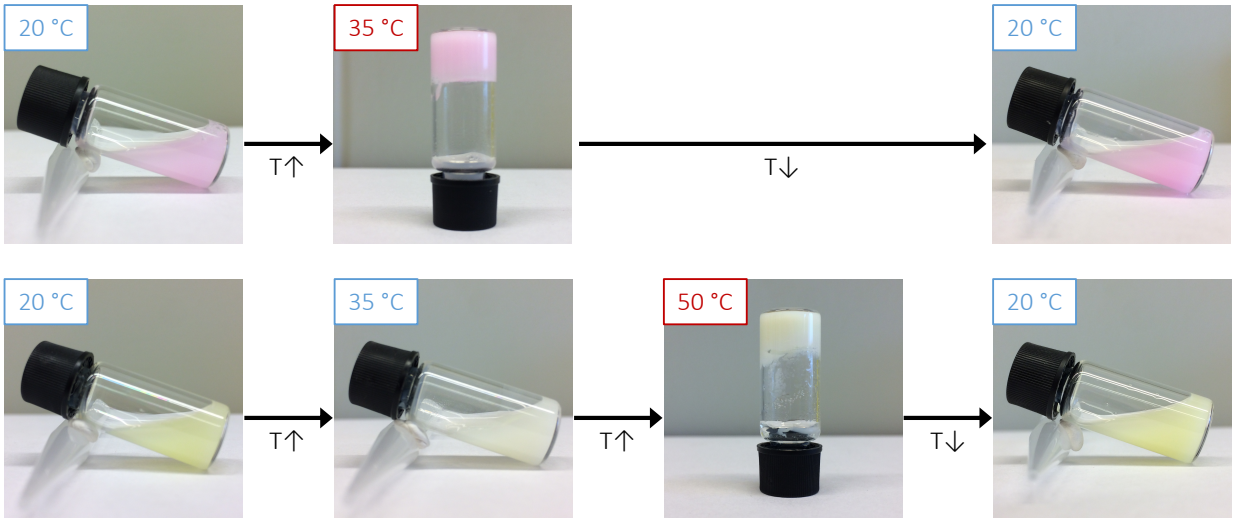

Figure S3: **(top panel)** PNIPAM-GMA and **(bottom panel)** PNIPMAM-GMA suspensions undergo a reversible liquid-to-gel transition when the VPTT is crossed, here demonstrated with 1.7 wt% PNIP(M)AM-GMA in 100 mM KCl and 1 mM HCl.

Sequential Gelation in a Binary Mixture of PNIPAM-GMA and PNIPMAM-GMA

In a binary mixture of PNIPAM-GMA and PNIPMAM-GMA, since the repulsive-to-attractive transition occurs at lower temperatures for the PNIPAM-GMA than for the PNIPMAM-GMA, a volume-spanning core-shell-type network with a PNIPAM microgel core and a PNIPMAM microgel shell forms as a result of sequential gelation as the temperature is raised (Fig. S4).

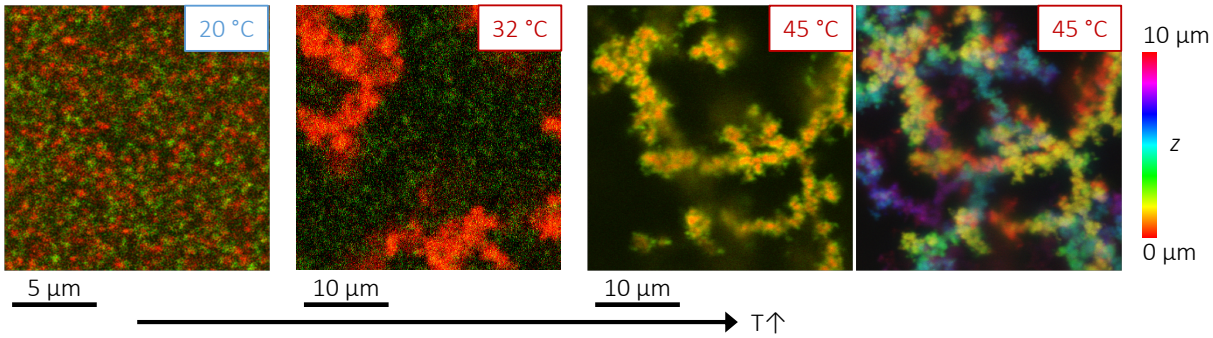

Figure S4: *xy* CLSM micrographs recorded in a mixture of 1.0 wt% PNIPAM-GMA and 1.0 wt% PNIPMAM-GMA in 100 mM HCl, at **(left)** 20, **(middle)** 32 and **(right)** 45 °C together with **(far right)** a corresponding color-coded *z* stack consisting of 30 *xy* frames.

Droplet Device Design

Computer-aided design (CAD) drawings of the short and long droplet devices, together with micrographs showing some characteristic features of the devices, are shown in Fig. S5A-C and D-F, respectively. Both devices have planar flow-focussing geometries[4–6] and square droplet generation cross sections of 10 μm. With experiments conducted at low capillary numbers ($Ca = \frac{U\mu}{\gamma} \lesssim 0.1$, with U being the characteristic velocity, μ the dynamic viscosity, and γ the interfacial tension), droplets are expected to form in squeezing and dripping mode. In these modes the droplet diameter d is expected to scale as $d/D_H \sim Ca^{\frac{1}{3}}$.[7,8] As a result, a droplet size close to the size of the droplet generating constriction, 10 μm (corresponding to a volume of $\sim$ 0.2 pl), is expected. Here, the hydraulic diameter D_H is given by $D_H = 4A/P_w$, where A is the cross sectional area of the constriction and P_w the perimeter of the cross section.

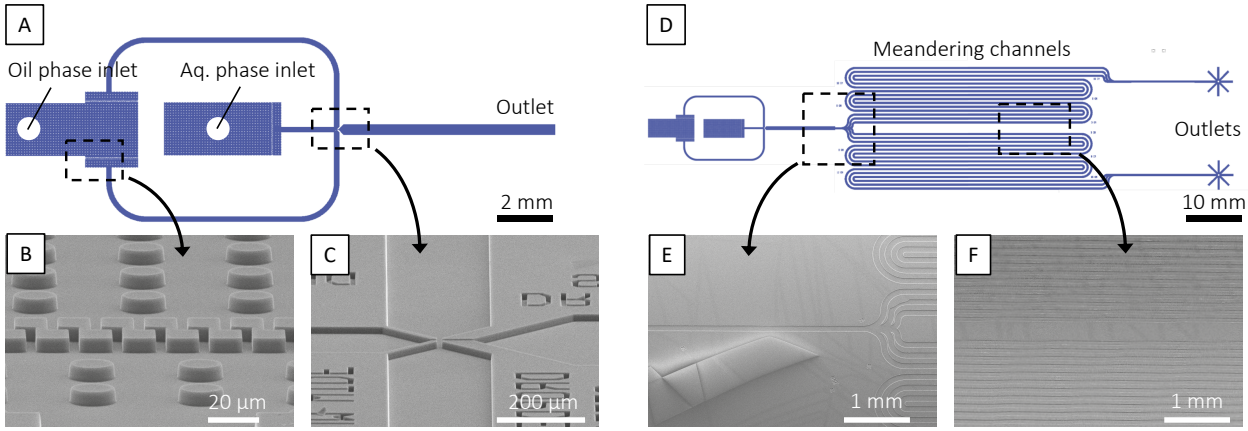

Figure S5: The two droplet devices used in the current study. **(A)** CAD drawing of the short, high generation frequency droplet device. This device contains an inlet for each phase and a single outlet. **(B)** Both inlets are equipped with a sieving structure where unwanted particles that can potentially clog the device are removed. **(C)** The oil phase and the aqueous phase meet at the constriction where droplets are formed. **(D)** CAD drawing of the long, meandering droplet device. The first section is identical to that of the short device. **(E-F)** Downstream with respect to the constriction, six meandering channels have been added to enable on-chip observation of the droplet shrinking process.

Fluidic Simulations of Droplet Devices

COMSOL 5.3 was used to carry out computational fluid dynamics (CFD) simulations in order to estimate the pressure drop distributions and the hydraulic resistances of the different devices used in this study. The CAD drawings of the short and the long device was directly imported into COMSOL and converted to a single block to enable CFD analysis. The finite element model was set up using the 2D Creeping Flow Module in the CFD Physics Toolbox. The inlet pressures were set to $P_{in} = 10$ Pa with an entrance length of 100 μm, while the outlets were set to $P_{out} = 0$ Pa. The mesh consisted of ∼200,000 elements and the PARADISO solver was used with standard settings. Water, incompressible, was used as the liquid from both inlets.

The results show that a significant part of the pressure drop across the devices occurs, as expected, over the droplet forming constriction (Fig. S6). At the same time, the pressure drop over this region for the short device (75% of total pressure drop) is much larger than that of the long device (10% of total pressure drop). A large pressure drop is beneficial as this means that a large part of the energy put into the system acts to form droplets (i.e. to create new interface between the oil and the water phase). With a larger pressure drop at the constriction, a higher droplet generation frequency or smaller droplets can be expected at the same driving pressure applied to the device.

The resistance measurements further point to how the shorter device is better suited for high frequency droplet generation. Here, the hydraulic resistance of the short device is $R_{short} = 3.9 \times 10^{14}$ Pa·s·m^{-3} while the resistance of the long device is about 24 times as high, $R_{long} = 9.4 \times 10^{15}$ Pa·s·m^{-3}.

The length of the meandering channels is ∼45 cm. This means that if we want a residence time of 5 min, the average flow velocity should be ∼1.50 mm/s. In our model, the corresponding pressure drop across the device to achieve this flow velocity is 84,000 Pa (840 mBar).

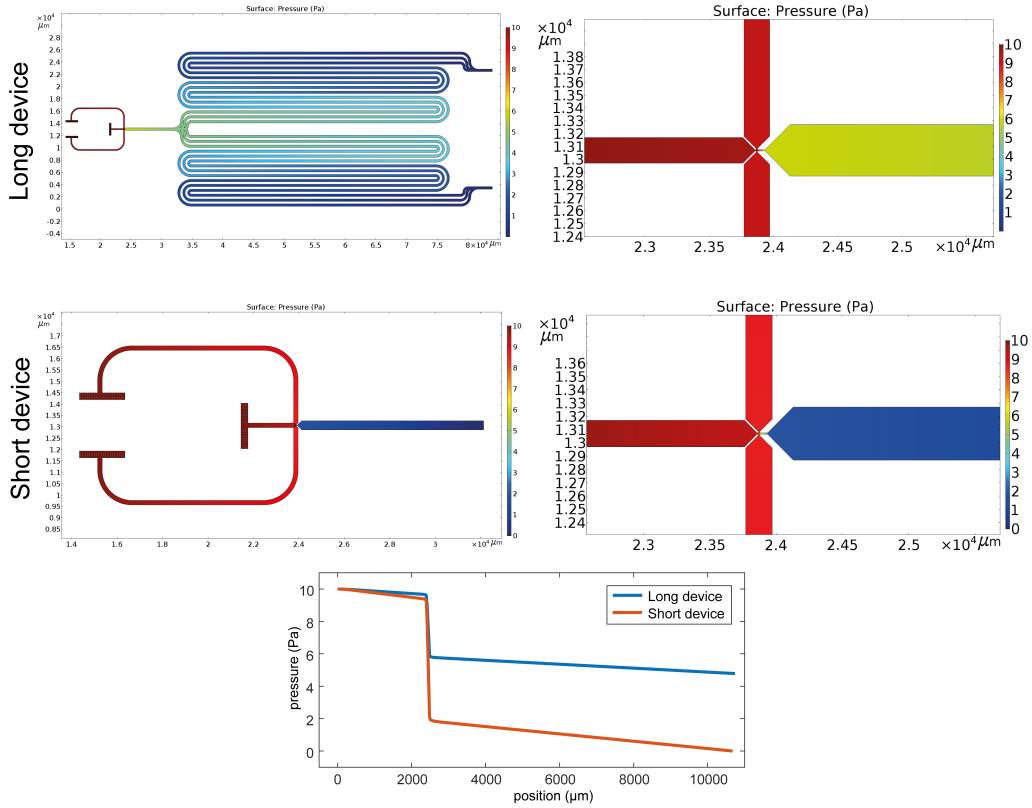

Figure S6: Comparison between pressure drop in **(top)** the long and **(middle)** the short device using COMSOL Multiphysics to simulate the flow field. The inlet pressures were set to 10 Pa, the outlet pressure to 0 Pa. **(bottom)** For the long device only ∼10% of the pressure drop occurs at the droplet constriction while the corresponding number for the short device is ∼75%. The distance over which this was measured corresponds to the distance between the aqueous phase inlet and the outlet of the short device.

Droplet Diameter and Generation Frequency as a Function of Oil and Aqueous Phase Pressure

At a constant aqueous phase pressure (500 mBar) the droplet diameter decreases exponentially to around the size of the constriction (10 μm) with increasing oil phase pressure (Fig. S7, left). The size reduction is expected since a higher oil pressure decreases the time it takes to pinch off the water thread and create a droplet. The minimum droplet diameter is comparable to the constriction size due to the device operating in squeezing mode. The droplet generation frequency is naturally linked to the droplet diameter. At low

oil pressures the mean droplet diameter is very large, and as a consequence the generation frequency is low. At the highest oil pressures, the generation frequencies are low due to the oil phase reducing the water phase flow rate. Consequently, the maximum generation frequency is reached at intermediate oil phase pressures, comparable to the water inlet pressure.

When keeping the oil phase pressure constant (500 mBar) while varying the aqueous phase pressure, an increase in the droplet diameter with increasing pressure is observed (Fig. S7, right). This is expected since a higher water pressure allows for generating larger droplets before being pinched off by the oil phase. With increasing water pressure the droplet generation frequency seems to follow a similar trend as for the previous study. Low water phase pressure results in low generation frequency as the higher oil pressure hinders the water from entering the constriction. At very high water phase pressures relative to the oil phase, the time to pinch off the water thread is extended significantly.

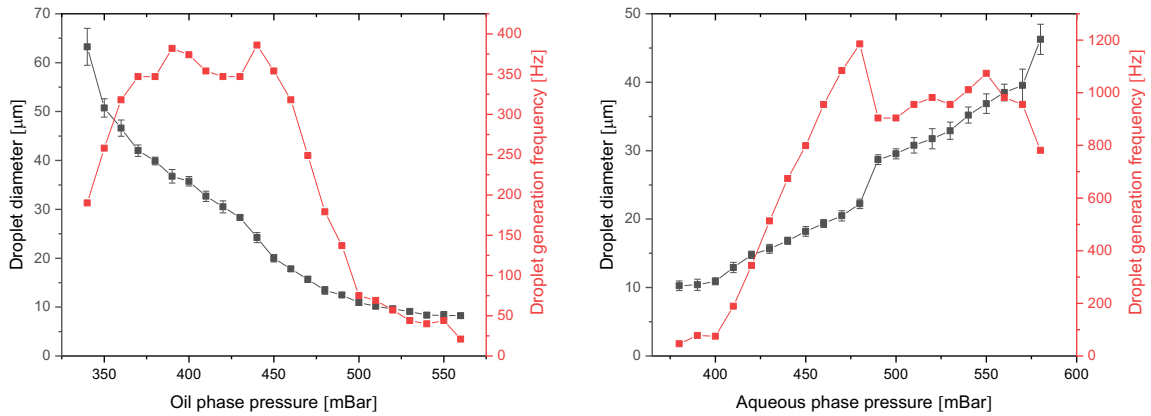

Figure S7: Droplet diameter and generation frequency as a function of varying either **(left)** the oil phase pressure or **(right)** the aqueous phase pressure while keeping the pressure of the other inlet constant at 500 mBar.

Droplet Flow Velocity

The water droplet flow velocity (Fig. S8) is not constant along the length of the device but is initially restricted due to droplet-wall friction effects.

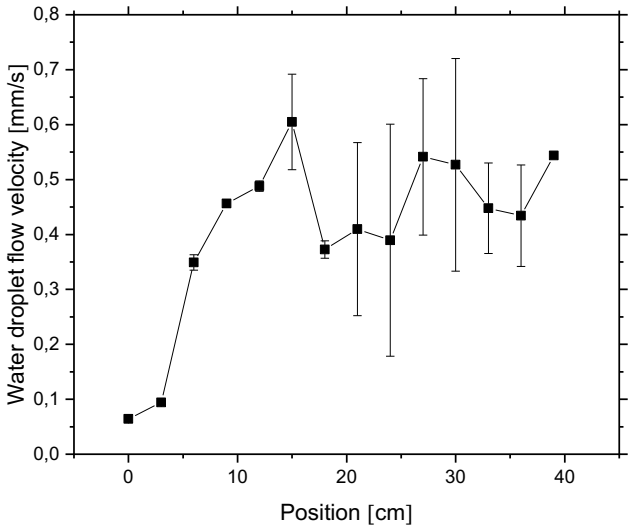

Figure S8: Water droplet flow velocity as a function of position in the meandering channel.

Droplet Diameter Analysis

For the droplet size analysis, an ImageJ 1.51n[9] script was developed which was able to correctly determine the droplet size of several thousands of droplets per second flowing in the straight, wide channel (Fig. S9). Typically, an image stack containing 500 frames acquired at 5,000 frames per second was used. Frame number 0, 50, 100,... 500 were selected for analysis in order not to image the same droplet multiple times, generating 11 frames of unique droplets. First, the background was subtracted by a rolling ball function with a radius equal to the radius of the droplets (7 pixels). Thereafter the images were thresholded to create a binary image stack; a grey scale range of 20-255 was used to select individual particles and to avoid overlap. In order to recreate the shape of droplets which had been distorted the binary function *Fill Holes* was used. Non-circular objects were then excluded by using the function *Analyze Particles* with the area range set to 0-∞ μm^2 and the circularity range set to 0-0.9; the selected areas were removed by filling them white. Next, objects too small to be droplets were excluded with the area range set to 0-35 μm^2 and the circularity range set to 0-1.0. Selected areas were once again filled white. Next, double *Dilate* operations were performed followed by *Watershed*. The diameters of the remaining

particles were measured by taking the mean of the major and minor axis of an ellipsoidal fit. In total, 10,653 droplets were measured.

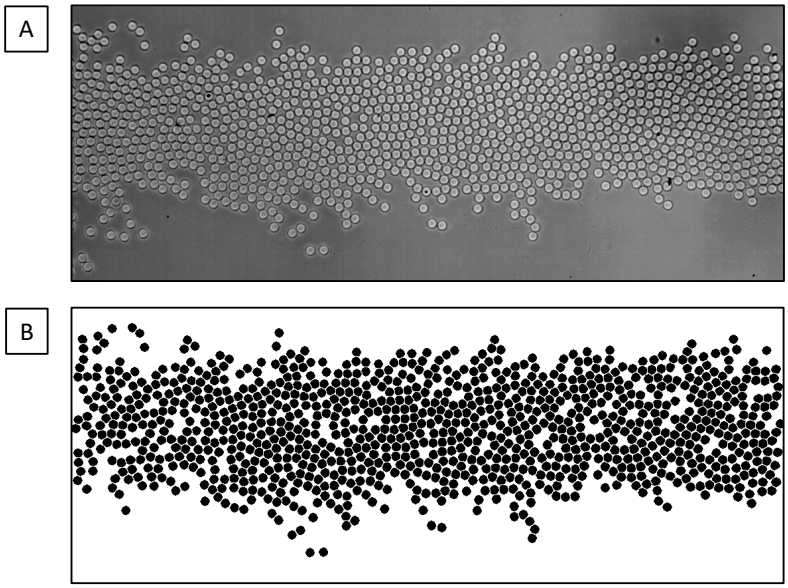

Figure S9: Automated image processing was used in order to determine the diameters of several thousands of droplets accurately. **(A)** Original image (770x297 μm). **(B)** Processed image with droplets to be analysed.

Video S1: Generation of Microgel-Containing Water Droplets in the Short Device

This video shows the encapsulation of PNIPAM microgels (i.e. the genration of microgel-containing W/O droplets) using the short device. The driving pressures are $P_w = 800$ mBar and $P_{oil} = 850$ mBar for the water and oil pressure respectively. The resulting droplet generation frequency is around 3,000 Hz. The oil used is HFE-7500 with 2 wt% PicoSurf 1. The droplet device is operating in squeezing mode where droplet breakup is to a large extent dependent on the geometry of the constriction where droplets are generated, as the aqueous thread blocks the oil phase creating a pressure build-up acting to pinch of a single droplet.

Poisson Distribution of the Number of Microgels per Droplet

A 0.00270 wt% PNIPAM-GMA suspension was used as aqueous phase in droplet generation experiments where the goal was to investigate the distribution of the number of microgels per water droplet. The distribution is expected to follow a Poisson distribution with a probability mass function (PMF) given by:

$$P(X = k) = \frac{e^{-\lambda}\lambda^k}{k!} \tag{1}$$

where $k = 0, 1, 2, 3, ...$, is the number of microgels per droplet and λ equals the mean of the distribution $E[X]$ according to:

$$E[X] = \lambda \tag{2}$$

Experimentally, however, the number of microgels per droplet could only be quantified (counted) after droplet shrinking (i.e. in the cluster state), this since individual microgels very rapidly diffuse in and out of the field of view in the large droplets and therefore cannot be counted properly. Naturally, empty droplets (containing zero microgels) eventually disappear as a result of water evaporation and the resulting clusters containing zero microgels obviously cannot be counted. Consequently, the experimentally determined distribution of the number of microgels per cluster is expected to follow a zero-truncated Poisson (ZTP) distribution with a PMF given by:

$$P(X = k|X > 0) = \frac{\lambda^k}{(e^\lambda - 1)k!} \tag{3}$$

with the truncation stipulated as $k > 0$, i.e. it is impossible for the variable k to be zero. For the ZTP, $E[X]$ is given by:

$$E[X] = \frac{\lambda e^\lambda}{e^\lambda - 1} \tag{4}$$

Following complete droplet shrinking, a total of 408 of the resulting clusters in oil were

visually inspected and the microgels in each cluster were counted. An arithmetic mean of 4.17 microgels per cluster was obtained. The distribution (number of microgels per cluster) was fitted with the ZTP (Eq. 3) giving $\lambda_{cluster} = 4.044$. Insertion of this value into Eq. 5 gave $E[X]_{cluster} = 4.12$. The discrepancy of the two means (4.17 and 4.12) is low due to the fact that the number of empty droplets is low, 1.8%. The fraction of empty droplets was calculated by applying the the Poisson recurrence formula:

$$P(X = x + 1) = \frac{\lambda}{x + 1} P(X = x) \tag{5}$$

to access P(X=0).

In order to test if our data follows the ZTP distribution we used the chi-square goodness of fit test with a null hypothesis H_0 that the data follows this distribution. The chi square test is then:

$$\chi^2_{k-2} = \sum_k \frac{(f_0 - f_e)^2}{f_e} = 2.38 \tag{6}$$

where f_o is the observed frequency, f_e the expected frequency under ZTP, k the number of possible outcomes (microgels per droplets) with an expected frequency larger than 1 (in these measurements the value was $k = 10$). With a 0.05 level of significance and a $k - 2 = 8$ degrees of freedom we get a percentage point of 15.51 for the chi-square distribution. Since $\chi^2 = 2.38 < 15.51$ the decision is to not reject H_0.

Completely Shrunken Droplets - Clusters in Oil

Examples of colloidal molecule-like microgel clusters in oil, formed as a result of water droplet shrinking, are shown in Fig. S10. Since the oil is a bad solvent for the microgels the clusters are very dense. This makes it somewhat difficult to distinguish individual microgels within a given cluster.

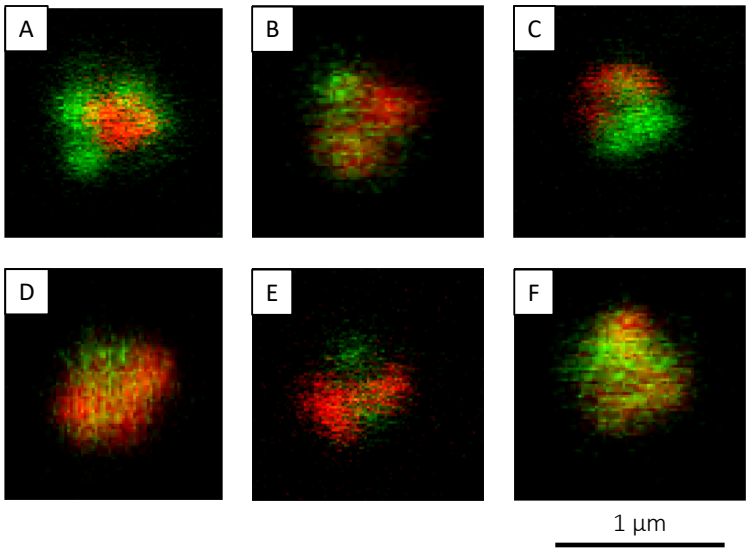

Figure S10: Zoomed-in CLSM micrographs of dense microgel clusters in oil, after complete evaporation of water from microgel-containing water droplets. PNIPAM-GMA and PNIPMAM-GMA microgels are labelled red and green, respectively.

Phase Transfer

Following crosslinking, the microgel clusters were transferred from oil into water by a series of washing steps to remove the oil and surfactants (protocol below). This initially proved difficult, with a relatively large fraction of the clusters retained in the oil phase. After multiple tries with the perfluorinated oil FC-40 as continuous phase, this oil was substituted for the semifluorinated oil HFE-7500. The greater solubility of HFE-7500 in organic solvents lead to more efficient oil removal and a more successful phase transfer. Furthermore, as water is more soluble in HFE-7500 compared to FC-40, droplet shrinking was faster.

Protocol: The oil-to-water transfer procedure builds on previous work by Abate, Han, Jin, Suo and Weitz.[10] First, 1 ml of 20 wt% perfluorooctanol (PFO) in oil is added to 500 µl of cluster suspension. The PFO acts as a demulsifier, breaking the emulsion by coalescing the dispersed aqueous phase while being vortexed for 1 min. Four rounds of washing are subsequently needed in order to remove the oil and surfactants. First, 5 ml 1 wt% Span-80 in hexane is added and vortexed for 1 min before centrifuging (Sigma 6K-15) at

3,000 rpm (1,830 g) for 15 min. Here, the top 6 ml is aspirated and discarded as the hexane has lowered the oil density below that of water. In the second round, 1 ml of pure hexane is added, and the sample is vortexed 1 min, then centrifuged (Biofuge pico) at 10,000 rpm (9,500 g) for 5 min. The top 1 ml layer is aspirated and discarded. In the third washing round, 1 ml 0.1 wt% Triton X-100 in water is added, and the sample is again vortexed for 1 min and centrifuged at 10,000 rpm (9,500 g) for 5 min. Also, 1 ml of the top layer is aspirated and discarded. The last round of washing is with 1 ml Milli-Q water, again vortexed for 1 min, centrifuged at 10,000 rpm (9,500 g) for 5 min, and 1 ml of the top layer is discarded. The result is 500 µl of dilute aqueous cluster suspension.

Video S2: Association of Microgel Clusters at Elevated Temperature

Colloidal molecule-like microgel clusters in water were imaged by CLSM at 35 °C (100 mM KCl and 1 mM HCl). At this temperature the PNIPAM-GMA microgels display attractive behavior wheres the PNIPMAM-GMA ones are repulsive. Video 2 shows the attraction-induced association of three small aggregates (in turn formed by association of small clusters), in bright field (left) and fluorescence mode (right), respectively. Frame rate is 15 fps.

References

1. Reis, A. V.; Fajardo, A. R.; Schuquel, I. T.; Guilherme, M. R.; Vidotti, G. J.; Rubira, A. F.; Muniz, E. C. Reaction of Glycidyl Methacrylate at the Hydroxyl and Carboxylic Groups of Poly(Vinyl Alcohol) and Poly(Acrylic Acid): Is This Reaction Mechanism Still Unclear? *J. Org. Chem.* **2009**, *74*, 3750–3757.

2. Huang, G.; Gao, J.; Hu, Z.; John, J. V. S.; Ponder, B. C.; Moro, D. Controlled Drug Release from Hydrogel Nanoparticle Networks. *J. Controlled Release* **2004**, *94*, 303–311.

3. Shah, R. K.; Kim, J.-W.; Weitz, D. A. Monodisperse Stimuli-Responsive Colloidosomes by Self-Assembly of Microgels in Droplets. *Langmuir* **2009**, *26*, 1561–1565.

4. Anna, S. L.; Bontoux, N.; Stone, H. A. Formation of Dispersions Using 'Flow Focusing' in Microchannels. *Appl. Phys. Lett.* **2003**, *82*, 364–366.

5. Gañán-Calvo, A. M. Generation of Steady Liquid Microthreads and Micron- Sized Monodisperse Sprays in Gas Streams. *Phys. Rev. Lett.* **1998**, *80*, 285–288.

6. Baroud, C. N.; Gallaire, F.; Dangla, R. Dynamics of Microfluidic Droplets. *Lab Chip* **2010**, *10*, 2032–2045.

7. Lee, W.; Walker, L. M.; Anna, S. L. Role of Geometry and Fluid Properties in Droplet and Thread Formation Processes in Planar Flow Focusing. *Phys. Fluids* **2009**, *21*, 032103.

8. Rosenfeld, L.; Lin, T.; Derda, R.; Tang, S. K. Review and Analysis of Performance Metrics of Droplet Microfluidics Systems. *Microfluid. Nanofluid.* **2014**, *16*, 921–939.

9. Schindelin, J.; Arganda-Carreras, I.; Frise, E.; Kaynig, V.; Longair, M.; Pietzsch, T.; Preibisch, S.; Rueden, C.; Saalfeld, S.; Schmid, B. *et al.* Fiji: An Open-Source Platform For Biological-Image Analysis. *Nat. Methods* **2012**, *9*, 676–682.

10. Abate, A. R.; Han, L.; Jin, L.; Suo, Z.; Weitz, D. A. Measuring The Elastic Modulus Of Microgels Using Microdrops. *Soft Matter* **2012**, *8*, 10032–10035.